1984ApJ...286..337F

THE ASTROPHYSICAL JOURNAL, **286**: 337–349, 1984 November 1

SHOCK WAVES IN MIRA VARIABLES. I. EMISSION-LINE SPECTRA

M. W. FOX, P. R. WOOD, AND M. A. DOPITA
Mount Stromlo and Siding Spring Observatories, Research School of Physical Sciences,
Australian National University

Received 1984 February 28; accepted 1984 May 18

ABSTRACT

A catalog of Balmer emission-line profiles (Hγ, Hδ, Hζ, and Hη) is presented for a sample of nine Mira variables ranging in period from 150 to 394 days. These were obtained at very high dispersion with phase coverage of about half a cycle centered around maximum. Observations of emission lines of Mg, Si, and Fe are also described. Variations with phase and cycle number of line profile shape and flux are discussed in relation to a simple shock model in which a spherically symmetric shock wave is propagating outward through the atmosphere of a pulsating Mira variable. From the simple shock model, estimates are made for the shock speed and postshock temperature at phases during which the Balmer emission lines are visible.

Subject headings: line profiles — shock waves — stars: long-period variables — stars: pulsation

I. INTRODUCTION

Emission lines of the hydrogen Balmer series are prominent in the spectra of Mira variables around maximum light. Since the work of Gorbatskii (1961), these features have been interpreted as due to heating of the stellar photosphere by a spherical shock wave propagating outward. To date there has been neither a satisfactory quantitative model for the production of Balmer line emission in Mira variables, nor a sufficiently accurate set of observational data with which model line emission may be compared. Existing analyses of spectral observations (e.g., Merrill 1945, 1946*a*, *b*, 1947*a*, *b*; Joy 1947, 1954; Maehara 1971) concentrate on the mean radial velocities of emission lines; there is very little published quantitative data on line shapes, widths, and intensities. Here we present these quantities for the hydrogen Balmer emission lines Hγ, Hδ, Hζ, and Hη in nine Mira variables of spectral type M, ranging in period from 150 days (S Car) to 394 days (W Vel). Phase coverage is typically one-third to one-half of a cycle around maximum light.

One of the outstanding problems concerning the Mira variables is their mode of pulsation (Wood 1982; Willson 1982). The case for fundamental mode pulsation (Hill and Willson 1979; Willson, Wallerstein, and Pilachowski 1982) relies heavily on a comparison of observed radial velocities of line spectra in Mira variables with simple (isothermal) models for shock propagation. However, Wood (1980, 1982) has analyzed these results and has shown that uncertainties in both the existing observational data and theoretical models make mode identification by this method essentially impossible at present. The observations presented herein, combined with detailed shock models (to be described in Paper II of this series, Fox and Wood 1984), should lead hopefully to a mode identification in which some confidence can be placed.

In the following section, the observations and data reduction are described. Qualitative features of the line spectra are presented in § III. Finally, in § IV, some explanations are offered for the nature of the emission-line spectra in terms of a simple model of the atmosphere of a pulsating Mira variable.

II. OBSERVATIONS

The line spectra displayed here were obtained with the coudé echelle spectograph and 81 cm camera on the 1.88 m telescope at Mount Stromlo Observatory. The one-dimensional Photon Array (PCA) (Stapinski, Rodgers, and Ellis 1981) was used as detector and a resolution of 0.025 Å pixel^{-1} was achieved, with a spectral range of 25 Å in each echelle order. The Balmer lines observed were Hγ (4340.46 Å), Hδ (4101.73 Å), Hζ (3889.05 Å), and Hη (3835.38 Å). In addition, several observations were made of emission lines of heavier elements (Mg, Si, and Fe), including at phases around minimum light. Most observations were made from 1978 July to 1979 February, with supplementary observations from 1982 November to 1983 June. Phases of the pulsation cycle were determined for each variable from visual light curves kindly supplied by F. M. Bateson, Variable Star Section, Royal Astronomical Society of New Zealand. Where no such observations were available, phases were derived from the predicted AAVSO maxima.

The objects in the sample are listed in Table 1. Included for each star are the period (Kukarkin *et al.* 1969), the spectral type at maximum (Keenan, Garrison, and Deutsch 1974), the heliocentric stellar center-of-mass velocity v_*, and the distance. The velocities were obtained from the midpoint of the twin OH maser emission features or from the midpoint of the molecular emission of thermally excited CO or SiO. This system of deriving stellar center-of-mass velocities was originally described by Reid and Dickinson (1976) and the velocities should be accurate to 1–2 km s^{-1}. For the stars without direct estimates of v_*, we have adopted the values of v_* given in parentheses in Table 1. These were chosen simply to give the same position of the hydrogen lines relative to the rest wavelength as found for the stars with known v_*, and such estimates are probably accurate to around 4 km s^{-1}. Distances were estimated by comparing the mean *K* magnitude of each star (Catchpole *et al.* 1979) with the mean absolute *K* magnitude for a star of similar period (Robertson and Feast 1981).

Calibration of the spectra to absolute flux was made to provide an additional quantitative test for the theoretical models of Paper II. The Hayes-Latham flux standards, three of which were observed over 1978–1979, are all early-type stars, so that the listed flux calibrations (Berger 1976 and references therein) specifically avoid the regions around the Balmer lines. To overcome this problem, model atmospheric line profiles (Mihalas 1966; Kurucz 1979) were used to interpolate between calibrated points. Selection of the appropriate model atmo-

TABLE 1

THE MIRA VARIABLES OBSERVED

Star	P (days)	Sp.	V_* (km s^{-1})	D (pc)
S Car	150	M0e	(297)	588
T Col	225	M5e	(59)	593
RR Sco	280	M6e	(−37)	251
R Aql	284[a]	M6.5e	30[b]	205
R Car	309	M5e	(17)	139
o Cet	332	M5.5e	56.5[c]	77
RR Sgr	334	M6e	89.5[d]	280
S Scl	366	M6e	(22)	308
W Vel	394	M7e	4[e]	340

[a] Period is decreasing.

[b] V_* (heliocentric) from the midpoint of the two OH maser peaks (Wilson and Barrett 1972) and from the center of the SiO thermal emission (Morris *et al.* 1979).

[c] V_* from the midpoint of the CO thermal emission (Knapp *et al.* 1982).

[d] V_* from the midpoint of the two OH maser peaks (Fillet, Foy, and Gheudin 1973).

[e] V_* from the midpoint of the two OH maser peaks (Bowers and Kerr 1977).

sphere was made from the observed *uvby* colors (Hauck and Mermilliod 1980). Absolute fluxes within the Balmer lines of the flux standards were obtained by fitting the model atmosphere continuum to the observations in Berger (1976). Photon count rates per unit received flux for multiple observations of the standards during each run were compared, in order to estimate the photometric accuracy of derived fluxes. Such comparisons indicate a formal error of 40% for the fluxes tabulated. The observed line fluxes (Table 2) typically vary by a factor of 40 in a single star over one cycle.

III. THE EMISSION-LINE SPECTRA

a) Hydrogen and Helium Lines

Observed line profiles for Hγ, Hδ, Hζ, and Hη are displayed for each star in Figures 1–9. Line profiles are plotted against velocity rather than wavelength since the emphasis here is given to the atmospheric kinematics of the Mira variables. A positive velocity corresponds to motion outward from the center of the star.

The main result shown by the present spectra is the change in the overall line shape and position with phase. When the hydrogen lines first appear in emission, the full base widths are around 80 km s^{-1} extending to ~40 km s^{-1} to either side of the stellar center-of-mass velocity, with the negative velocity emission about as strong as the positive velocity emission. As the phase increases, the emission on the negative velocity edge of v_* becomes relatively weaker so that for phases past maximum, the overall emission line shape (neglecting overlying line absorption) consists of two components: a Gaussian of FWHM ~30 km s^{-1}, centered 0–10 km s^{-1} more positive than v_* (the line center varies from star to star and from cycle to cycle), and a negative velocity wing of lower intensity

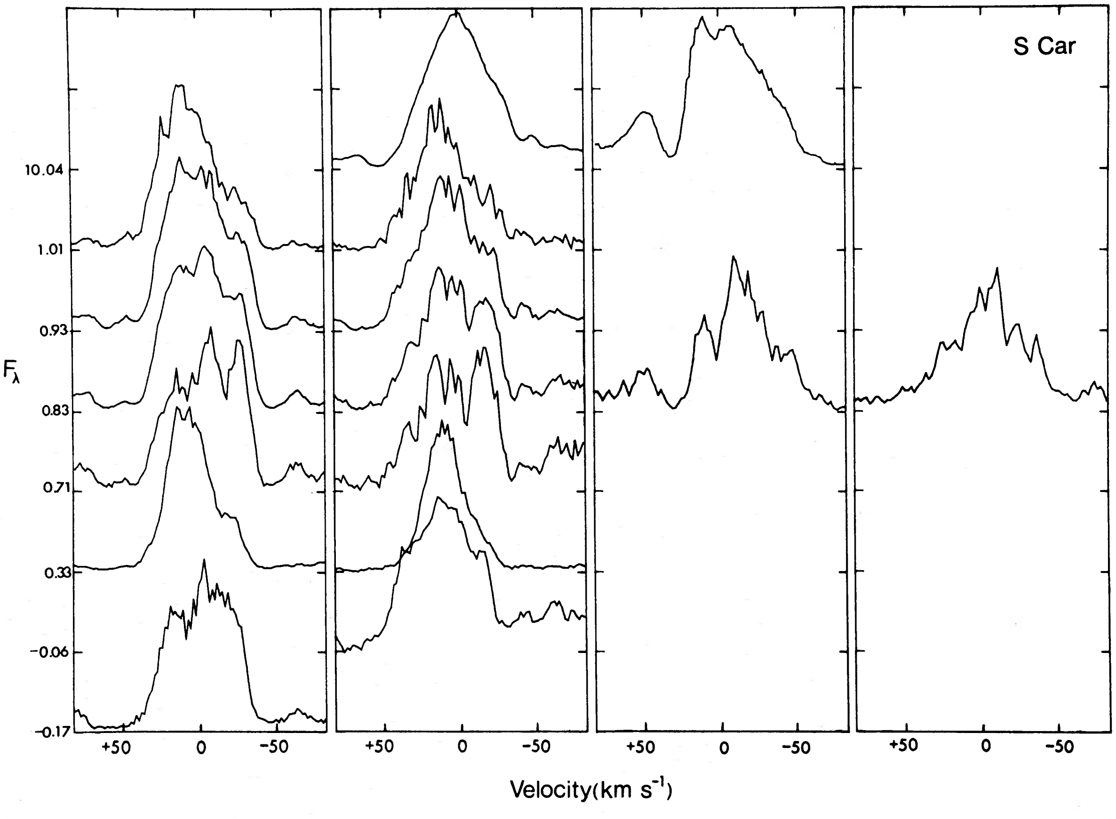

FIG. 1.—(*left to right*) Line profiles of Hγ, Hδ, Hζ, and Hη as a function of phase in S Car. F_λ is plotted vertically, with the zero flux level for each spectrum being indicated by a tick mark on the vertical axis. The phase of the observation is indicated next to each tick mark (phase 0.0 corresponds to the first maximum observed). Table 2 lists the maximum flux level in each line. The horizontal axis corresponds to wavelength on a logarithmic (i.e., velocity) scale (λ increases to the right). The line spectra have been positioned horizontally so that the line emission in the rest frame of the star will appear at the center of the plot (stellar center-of-mass velocities from Table 1 have been adopted).

1984ApJ...286..337F

TABLE 2

LINE FLUXES

STAR	PHASE	JD	Hγ		Hδ		Hζ		Hη	
			F_{peak}	F_{tot}	F_{peak}	F_{tot}	F_{peak}	F_{tot}	F_{peak}	F_{tot}
S Car	-.17	3729	3.1-11	2.2-11	-	-	-	-	-	-
	-.06	3747	-	-	4.0-12	4.0-12	-	-	-	-
	+.33	3805	4.2-11	2.2-11	4.2-11	2.0-11	-	-	-	-
	+.71	3862	1.6-11	1.2-11	7.5-12	6.2-12	-	-	-	-
	+.83	3879	1.4-10	1.0-10	9.7-11	7.0-11	3.1-11	2.5-11	2.8-11	1.8-11
	+.93	3884	7.2-11	5.7-11	5.4-11	3.9-11	-	-	-	-
	+1.01	3907	4.6-11	2.8-11	2.4-11	1.9-11	-	-	-	-
	10.04	5275	-	-	2.0-9	8.8-10	1.1-9	4.8-10	-	-
T Col	-.25	3714	2.8-12	2.2-12	6.5-12	3.3-12	-	-	-	-
	-.11	3747	1.8-11	9.5-12	3.9-11	2.0-11	1.3-11	6.1-12	2.1-11	1.3-11
	+.02	3775	4.9-11	2.8-11	9.9-11	4.9-11	4.3-11	2.0-11	2.3-11	1.1-11
	+.11	3795	8.5-12	5.0-12	1.8-11	7.1-12	9.1-12	3.6-12	-	-
	+.15	3804	1.5-11	5.0-12	2.7-11	1.0-11	1.1-11	4.6-12	6.9-12	2.8-12
	+.27	3831	2.3-12	1.0-12	3.5-12	1.4-12	-	-	-	-
	6.64	5275	-	-	2.5-11	8.3-12	1.0-11	3.8-12	1.6-11	5.6-12
RR Sco	-.04	3714	5.0-11	3.5-11	1.9-10	1.2-10	6.4-11	3.5-11	1.6-11	1.1-11
	+.02	3729	-	-	1.1-10	6.9-11	-	-	-	-
	+.08	3747	8.5-11	1.8-11	1.3-10	6.4-11	9.2-11	3.5-11	7.3-11	4.3-11
	+.18	3775	4.4-11	1.0-11	8.6-11	3.0-11	2.6-11	8.7-12	-	-
	+.25	3796	-	-	1.0-11	3.2-12	-	-	-	-
	+.29	3804	-	-	1.0-12	2.7-13	-	-	-	-
R Aql	-.12	3714	2.9-11	1.9-11	9.8-11	6.0-11	6.1-11	4.1-11	6.0-12	3.7-12
	-.07	3729	8.2-11	6.5-11	9.8-11	6.0-11	-	-	-	-
	-.01	3747	9.9-11	7.0-11	1.8-10	7.6-11	1.4-10	6.6-11	4.8-11	2.9-11
	+.08	3775	NE	-	NE	-	-	-	-	-
R Car	-.37	3715	1.0-12	4.8-13	1.8-12	4.4-13	-	-	-	-
	-.08	3805	1.3-10	9.6-11	2.1-10	1.3-10	-	-	4.4-11	4.9-11
	0.00	3832	-	-	-	-	2.1-10	1.1-10	-	-
	+.10	3861	2.0-10	1.1-10	4.7-10	1.8-10	2.1-10	7.5-11	8.7-11	5.6-11
	+.16	3882	1.1-10	4.1-11	5.5-10	1.9-10	3.1-11	1.1-11	9.5-11	3.9-11
	+.21	3894	9.0-11	2.9-11	1.0-10	2.9-11	3.0-11	1.0-11	2.7-11	6.7-12
	+.25	3907	8.0-11	2.7-11	7.0-11	1.9-11	2.9-11	6.1-12	6.9-12	1.2-12
	4.68	5275	-	-	9.4-10	1.6-10	2.2-10	4.6-11	3.1-10	5.4-11
	5.15	5420	3.5-11	6.1-12	6.3-11	1.1-11	3.4-11	6.5-12	3.3-11	7.2-12
o Cet	-.27	3747	-	-	NE	-	-	-	-	-
	-.18	3775	-	-	1.1-12	5.5-13	-	-	NE	-
	-.12	3795	3.8-12	2.9-12	3.2-12	1.7-12	-	-	5.6-12	7.0-13
	-.09	3804	2.6-11	2.2-11	5.0-12	2.9-12	1.5-11	6.8-12	4.3-11	8.3-12
	-.01	3831	1.8-10	1.3-10	1.1-10	5.7-11	1.3-10	5.5-11	5.7-11	2.7-11
	+.08	3861	1.2-10	8.9-11	1.8-10	8.4-11	1.7-10	5.9-11	7.2-11	2.7-11
	+.14	3882	1.4-10	9.3-11	5.6-10	2.1-10	3.0-10	1.1-10	6.3-11	2.5-11
	+.18	3894	8.4-11	4.5-11	5.1-10	2.0-10	4.9-11	1.7-11	-	-
	+.22	3907	3.0-11	1.5-11	1.2-10	3.8-11	-	-	-	-
	4.33	5275	-	-	1.7-9	3.9-10	1.2-9	2.7-10	9.0-10	2.1-10
	4.97	5487	8.9-9	5.0-9	1.1-8	4.9-9	NS	-	NS	-
RR Sgr	-.17	3714	NE	-	1.1-12	1.5-13	-	-	-	-
	-.07	3747	1.3-12	5.2-13	9.8-12	3.1-12	-	-	-	-
	+.02	3775	9.6-12	7.0-12	7.6-11	3.0-11	2.7-11	1.5-11	6.3-12	5.4-12
	+.08	3795	1.3-11	8.8-12	1.9-11	7.0-12	1.0-11	3.7-12	2.7-12	2.3-12
	+.10	3804	1.7-11	1.1-11	2.5-11	1.1-11	8.7-12	3.9-12	1.2-12	6.6-13
	+.18	3831	1.1-11	5.8-12	6.7-12	2.4-12	-	-	-	-
S Scl	-.24	3715	-	-	1.3-11	4.2-12	-	-	-	-
	-.15	3747	1.8-12	1.4-11	1.8-11	1.1-11	1.4-11	5.0-12	-	-
	-.07	3775	6.3-11	4.3-11	2.7-10	1.5-10	6.5-11	4.2-11	1.3-11	1.2-11
	-.02	3795	7.7-11	5.6-11	1.6-10	1.0-10	1.5-11	8.2-12	1.6-11	1.7-11
	+.01	3804	6.0-11	3.6-11	1.4-10	7.9-11	2.4-11	1.2-11	5.7-11	3.6-11
	+.08	3831	6.4-11	3.0-11	1.8-10	8.4-11	5.2-11	1.0-11	3.3-11	1.4-11
	+.16	3862	3.3-11	1.1-11	4.6-11	1.5-11	9.2-12	3.3-12	3.1-12	1.2-12
	+.21	3879	2.3-11	7.7-12	3.0-11	1.0-11	9.3-12	2.7-12	-	-
	+.25	3894	3.7-12	1.8-12	-	-	-	-	-	-
W Vel	-.11	3795	-	-	1.3-11	5.0-12	-	-	-	-
	-.09	3804	6.7-12	4.5-12	5.4-11	2.4-11	3.4-12	1.4-12	-	-
	+.05	3861	2.9-11	1.3-11	8.4-11	3.1-11	1.4-11	5.9-12	8.6-12	3.4-12
	+.10	3879	4.4-11	1.7-11	1.1-10	3.2-11	2.0-11	9.2-12	1.2-11	4.5-12
	+.14	3894	1.3-11	4.4-12	2.2-11	6.7-12	4.0-12	1.3-12	-	-

NOTES.—F_{peak} is the peak flux in the line in ergs cm^{-2} s^{-1} Å^{-1}. F_{tot} is the total flux in the line in ergs cm^{-2} s^{-1}. NE denotes no emission feature, and NS denotes no flux standard observed. JD is the Julian date minus 2,440,000.

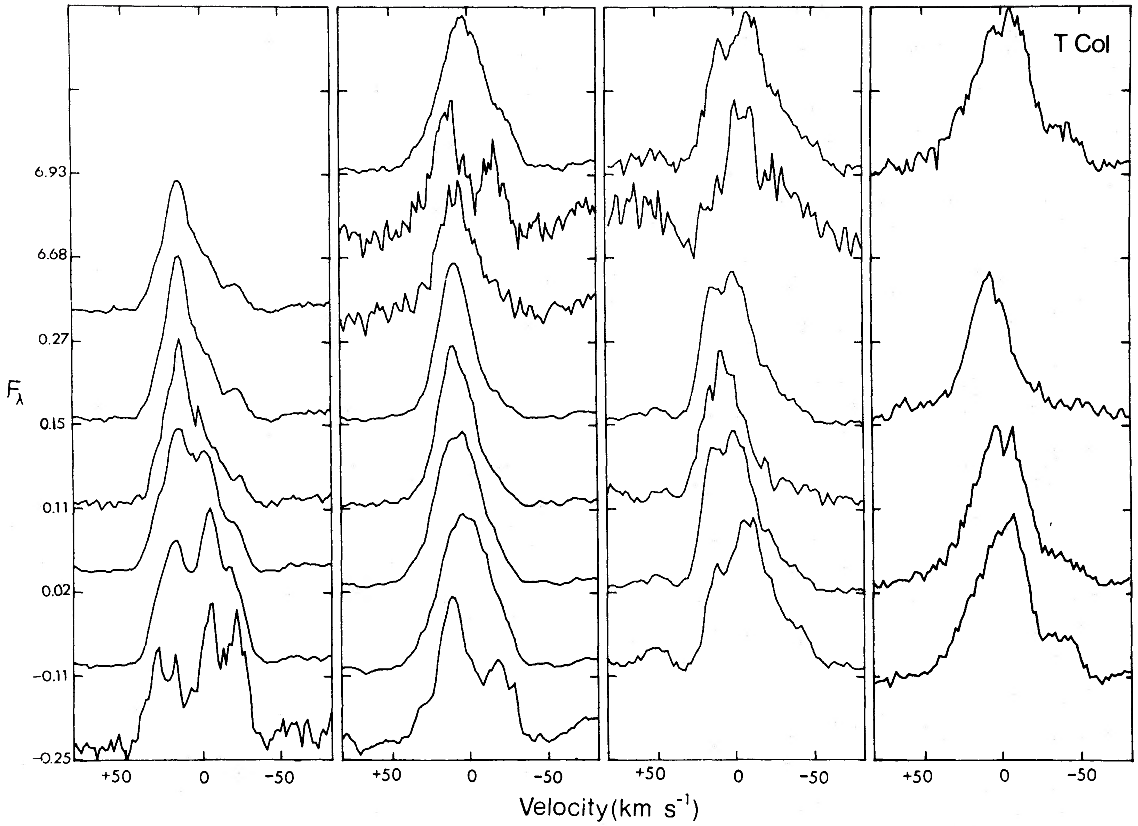

FIG. 2.—Same as Fig. 1 for T Col

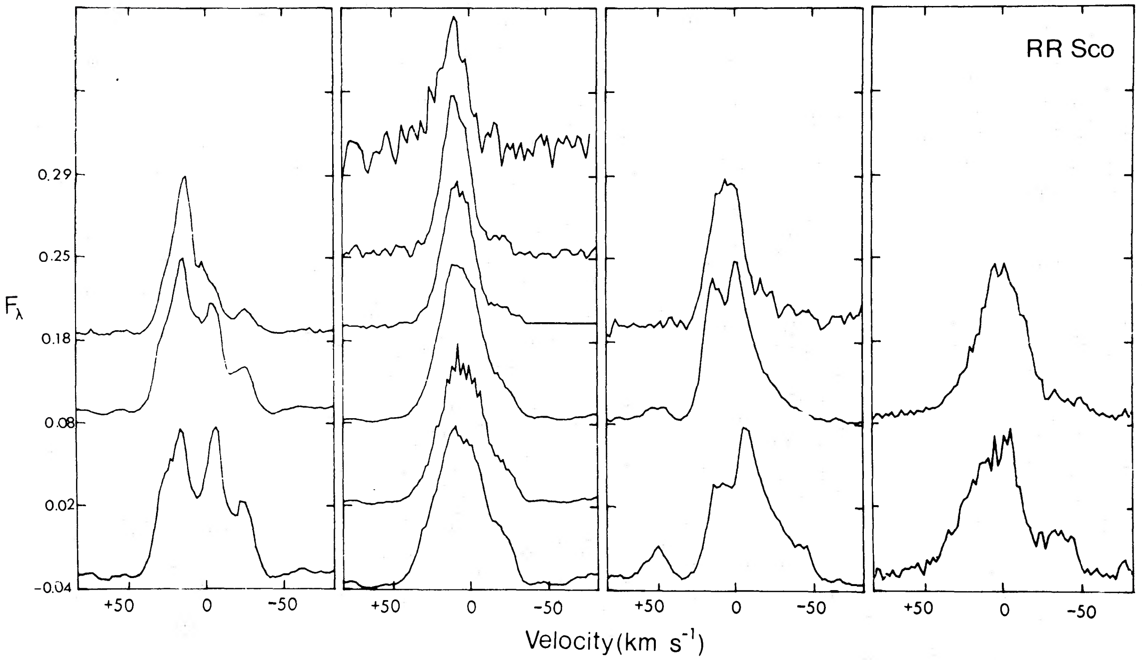

FIG. 3.—Same as Fig. 1 for RR Sco

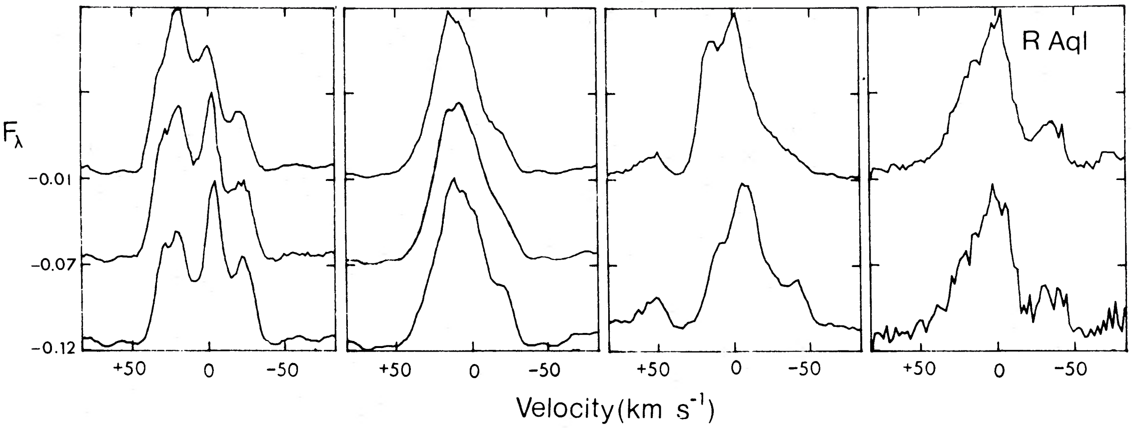

FIG. 4.—Same as Fig. 1 for R Aql

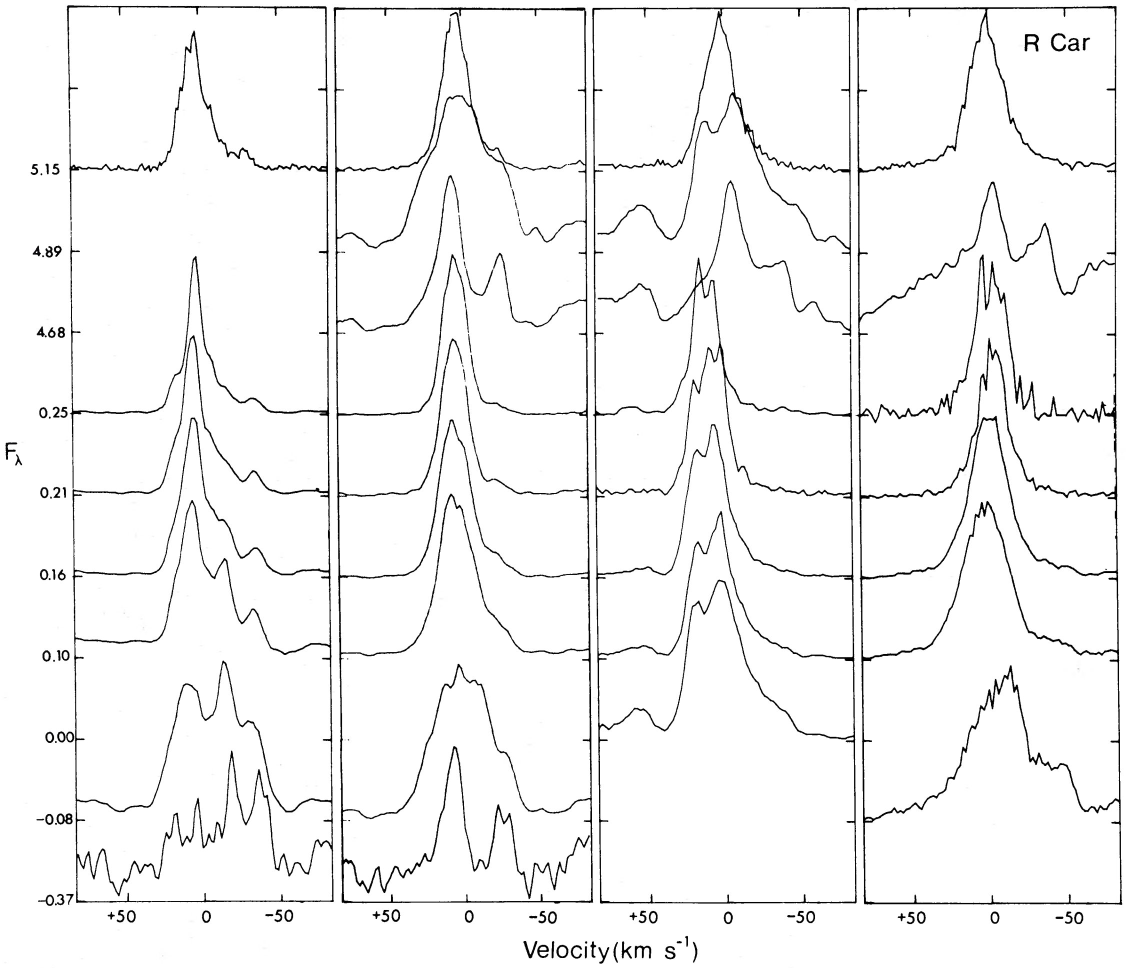

FIG. 5.—Same as Fig. 1 for R Car

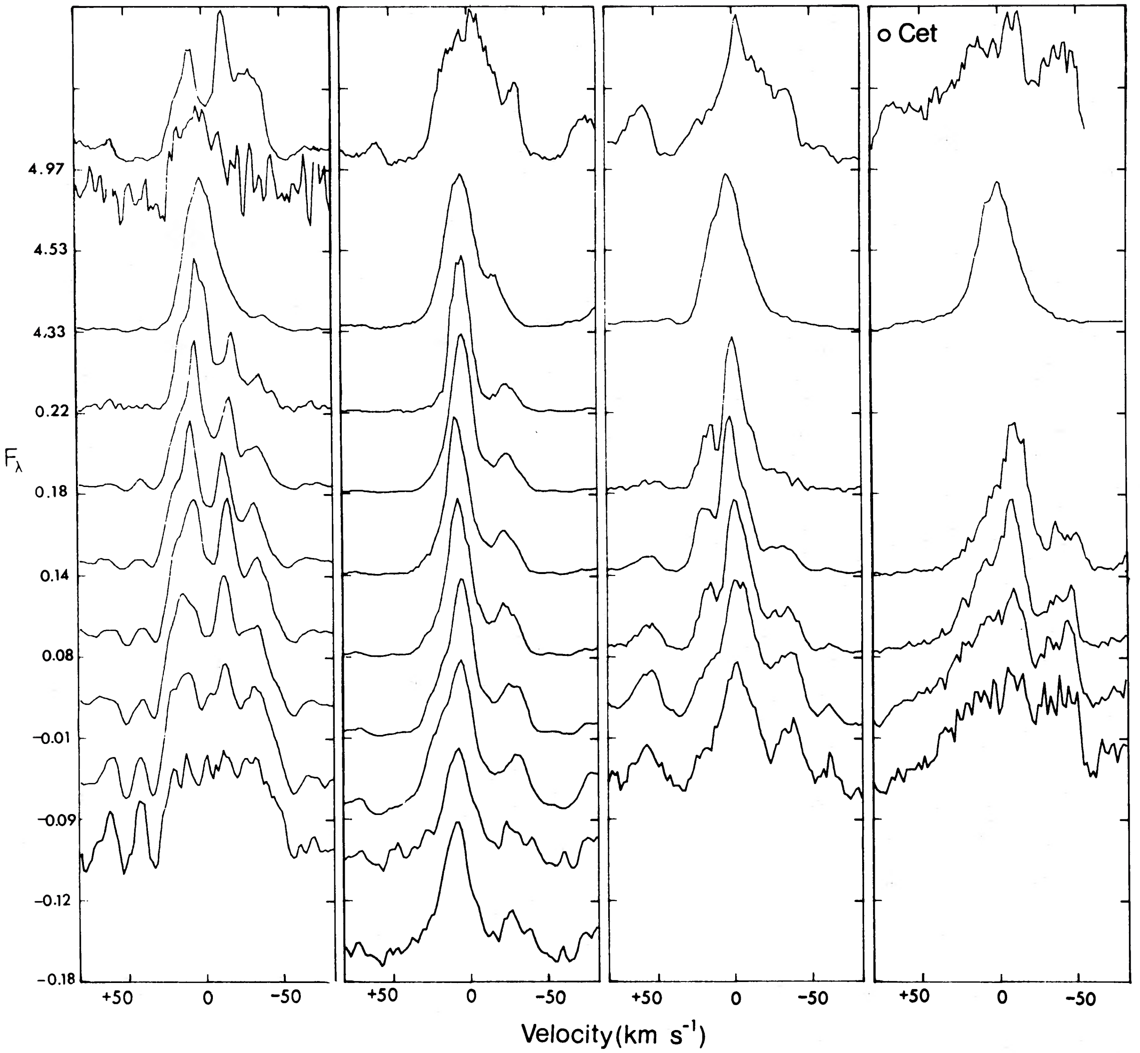

FIG. 6.—Same as Fig. 1 for *o* Cet

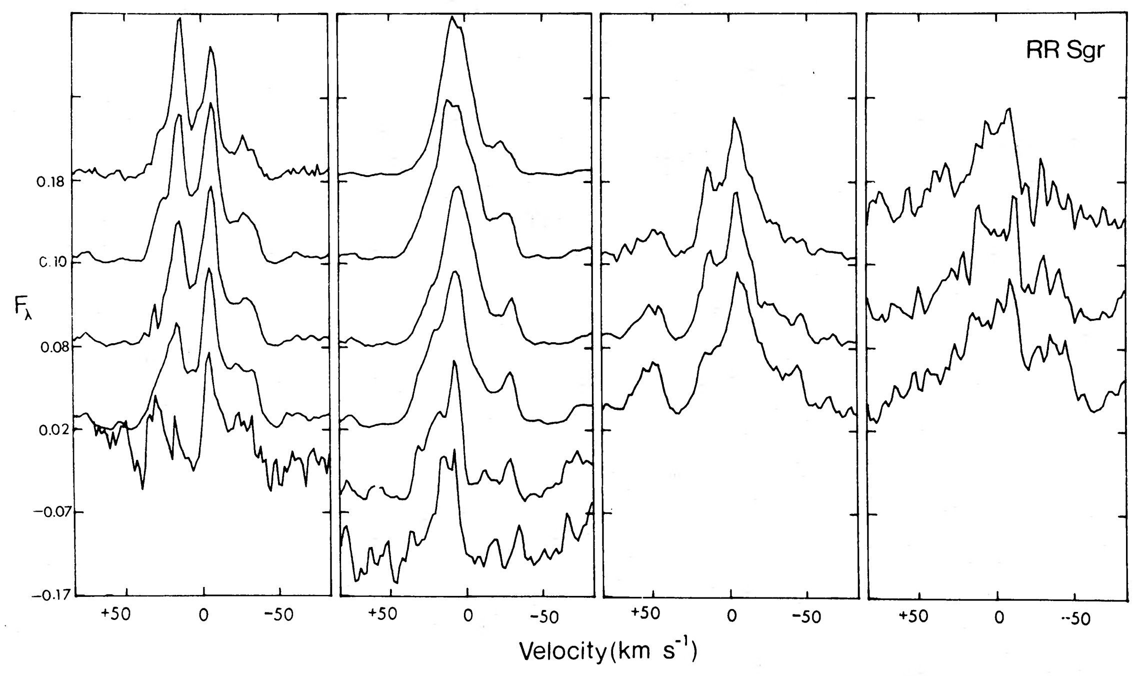

FIG. 7.—Same as Fig. 1 for RR Sgr.

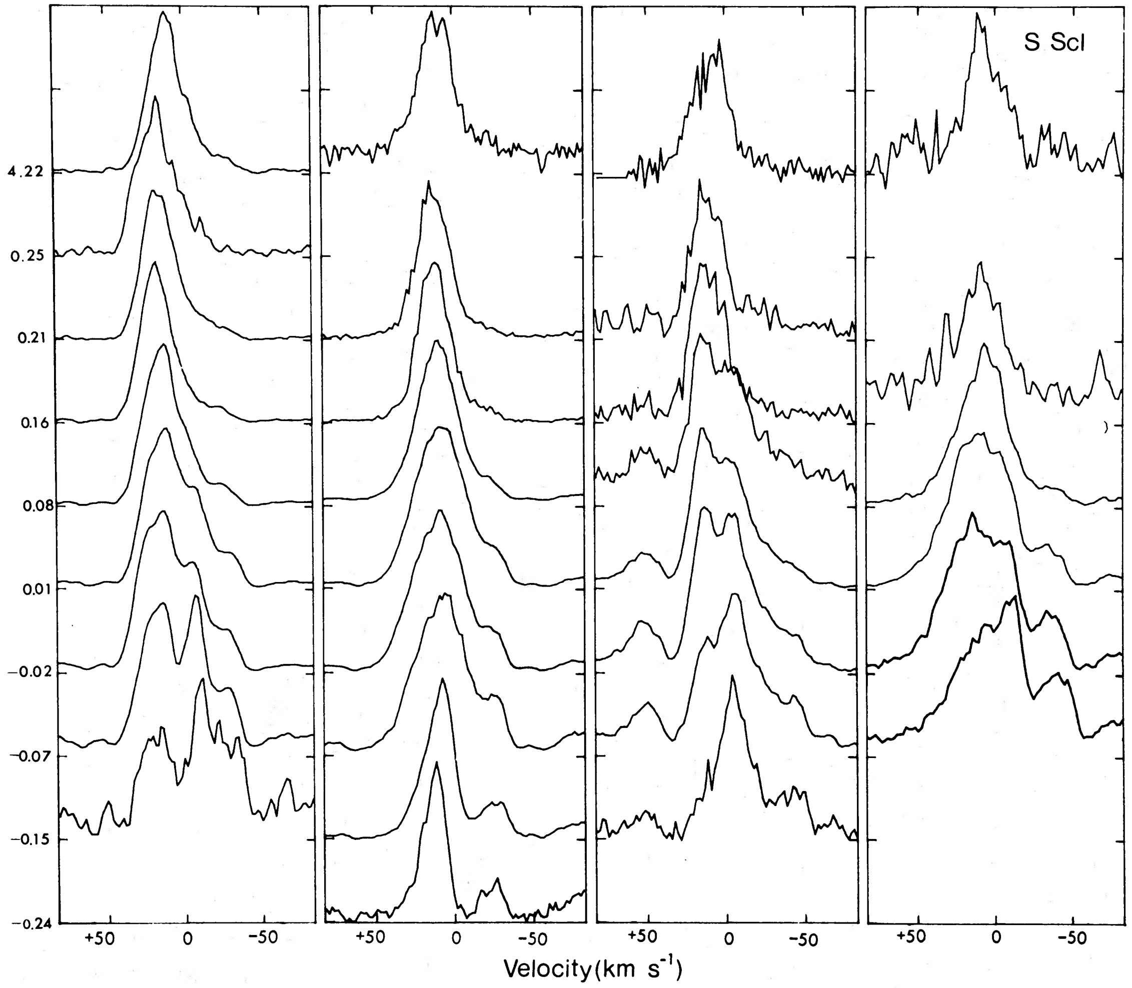

FIG. 8.—Same as Fig. 1 for S Scl

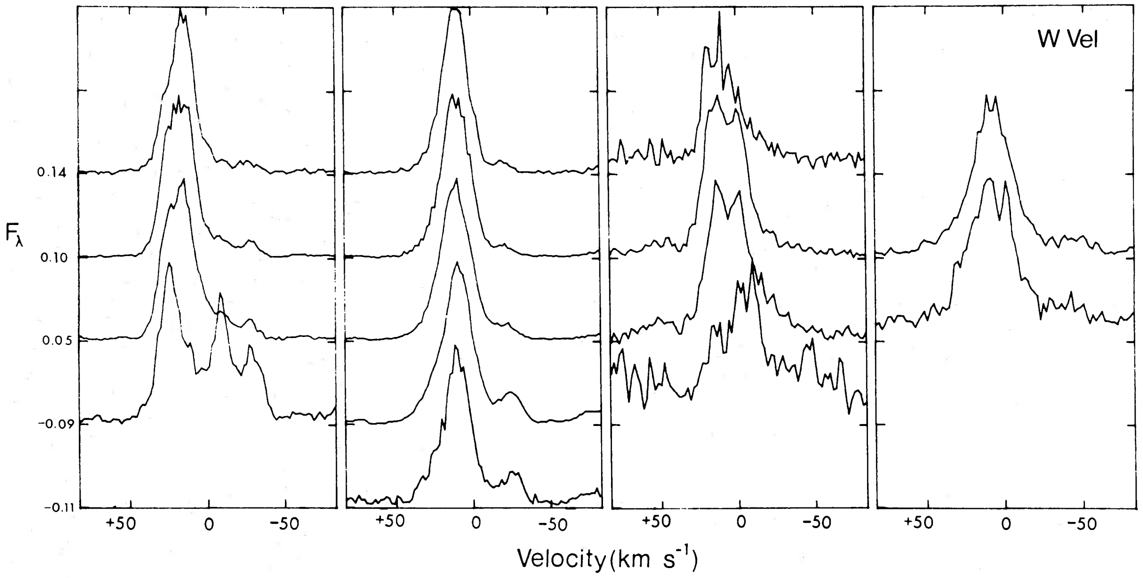

FIG. 9.—Same as Fig. 1 for W Vel

extending almost as far as the edge of the line at earlier phases. The position of the positive velocity edge of the line varies much less than that of the negative velocity edge. In addition to the features mentioned above, there is a general narrowing of the emission component with phase past maximum. In S Scl, the FWHM of the Gaussian component decreases from ~40 km s^{-1} to ~25 km s^{-1} at phase 0.2 while in R Car the corresponding variation is from ~55 km s^{-1} to ~25 km s^{-1}.

Before maximum the line shape is dominated by overlying absorption. As is well known, a number of atomic and molecular absorption lines are superposed on the Balmer emission lines, especially at early phases (Joy 1947). Strengths of the absorption features clearly vary from star to star. For example, they are strong in RR Sgr but fairly weak in S Scl. Line profiles from the two observed cycles of *o* Cet show that the absorption features can also vary greatly in strength from cycle to cycle. The maximum near JD 2,443,850 was particularly faint [V(max) ~ 4.6 mag compared with 3.4 on average], and the absorption lines were significantly stronger than in the later cycle. This result would be consistent with a weaker shock being formed at fainter maxima and not being able to propagate out through as much overlying material.

Another feature of the hydrogen line profiles worth examining is the consistency between different lines as regards line center and width. In general, at late phases, the profiles are almost identical in shape and position, indicating that there is little overlying absorption and that the lines are formed in the same region. However, notable exceptions do exist. For example, in W Vel the Hγ velocity appears ~5 km s^{-1} more positive than velocities of the other Balmer lines for phases past maximum. A similar shift of ~7 km s^{-1} is seen in Hζ in R Car in postmaximum phases. However, comparatively strong superposed absorption evident in Hγ in R Car suggests that perhaps absorption can account for the apparent shift in Hζ.

Prior to maximum light, although all lines are mutilated by overlying absorption, they have approximately the same full base widths and line centers. The one apparent exception to this is Hζ which appears to have an extended positive velocity emission edge (out to ~70 km s^{-1} compared to ~40 km s^{-1} for the other lines). This emission may be the $3p$–$2s$ line of He I at 3888.65 Å. The existence of this line in emission is consistent with the fact that Zirin (1976) has observed 10830 Å line of He I in emission in a number of Mira variables. The gap between Hζ and HeI 3888.65 is presumably due to Fe I 3888.52 in absorption.

b) Metal Lines

Each of the thermally excited metal emission lines Si I 4102.95, Mg I 3829.32, 3832.30, and 3838.29 were observed often because of their proximity to the hydrogen lines. The strength of these lines in emission varies considerably from star to star, being strongest in those stars with the greatest mutilation of the hydrogen lines by the overlying material (e.g., RR Sco). Some examples of the variations with phase in emission line profile of Si I 4102.95 and Mg I 3832.30 are shown in Figures 10 and 11 for *o* Cet and S Scl. In general, the positive velocity edges of these lines agree to within 3–5 km s^{-1} with the positive velocity edges of the hydrogen lines. However, the metal lines do not extend as far negative in velocity as the hydrogen lines because they lack the red wing associated with the latter.

Additional observations of metallic emission lines were obtained for *o* Cet at the late phase of 4.53 (i.e., near the

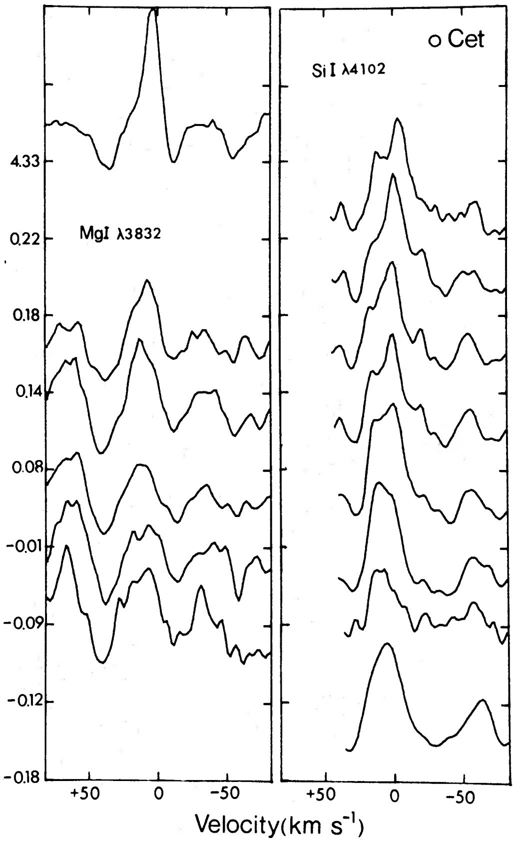

FIG. 10.—Same as Fig. 1 but for the lines Mg I 3832 and Si I 4102 in *o* Cet

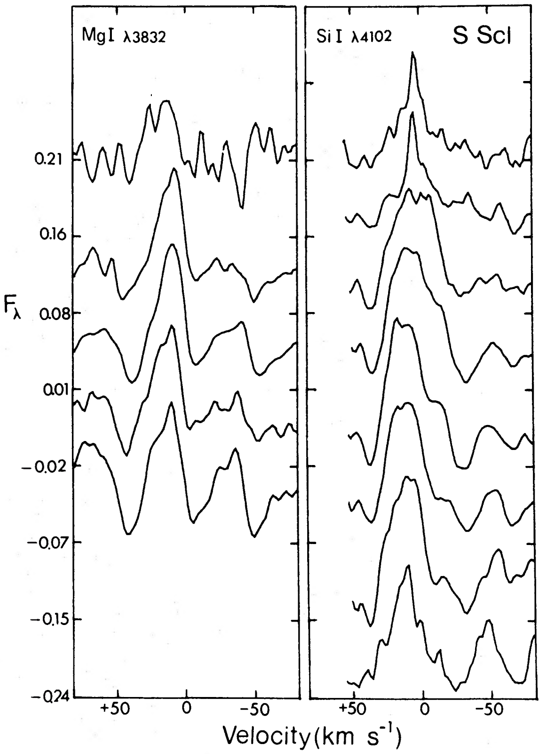

FIG. 11.—Same as Fig. 10 for S Scl

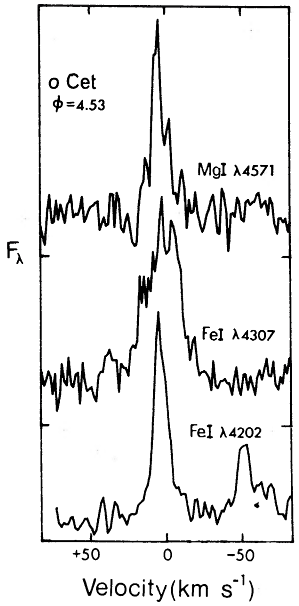

FIG. 12.—Same as Fig. 1 but for the lines Mg I 4571 and Fe I 4202, 4307 in *o* Cet at phase 4.53.

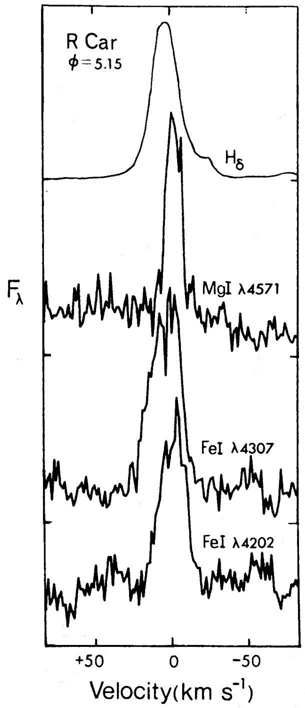

FIG. 13.—Same as Fig. 12 for R Car at phase 5.15

minimum four cycles after the first observed maximum) in order to get information on the velocity structure well after maximum (Fig. 12). At phase 4.53, the thermally excited line Mg I 4571.10 and the pumped line Fe I 4202.03 (pumped by Mg II 2795; Thackeray and Merrill 1936) are almost identical and have a FWHM of 14 km s^{-1} and a line center corresponding to an outward observed velocity of 4 km s^{-1} relative to Mira. However, Fe I 4307.91, from the same multiplet (42) as Fe I 4202.03, appears much broader than the other metallic lines, having a FWHM of ~28 km s^{-1}, although centered at the same velocity as the other lines. Given that the two Fe lines have the same upper state, their different widths are hard to explain. Two possible explanations are that rapid temporal variations may exist (the lines were observed 24 hours apart) or that there is emission from the Ti II line at 4307.90 Å. Neither explanation is convincing. Finally, we note that there is a suggestion of weak emission in Hγ at phase 4.53 in *o* Cet (see Fig. 6), this being an unusually late phase for hydrogen emission to appear.

The metal lines Mg I 4571.10, Fe I 4202.03 and 4307.91 were also observed in R Car at phase 5.15 (Fig. 13). In R Car, Mg I 4571 is narrow with FWHM of 13 km s^{-1}, while the two pumped Fe lines are broader (FWHM of 25 km s^{-1}—similar to that of the hydrogen lines at this phase). The Fe I and hydrogen lines also correspond very well in velocity, whereas Mg I 4571 is aligned with the negative velocity halves of the former lines. This indicates that there is a region with more positive velocity than the region giving rise to the thermally excited line Mg I 4571. The origin of these metallic emission lines will be discussed further in § V.

IV. LINE FLUXES

Using the method outlined in § II, fluxes in each of the Balmer lines, wherever visible, were computed and they are presented in Table 2. Included are the total flux observed as well as the peak intensity in the line. This latter can be used in conjunction with Figures 1–9 to get intensity through the line profile; tick marks on the ordinates denote zero intensity for each observation. Note that no correction for superimposed absorption lines has been made in calculating total line fluxes. This effect dominates at early phases.

Figures 14–16 display the phase variation of the fluxes listed in Table 2 for three of the most frequently observed stars. In all cases, variations were significantly greater than the formal errors cited earlier for these fluxes. Where phase coverage is best, fluxes in the Balmer lines vary over a factor of 40–50 from premaximum to postmaximum. Line fluxes peak in general on or around maximum visible light (−0.05 to +0.05). The line flux is clearly correlated with the relative strength of the cycle as measured by V_{max}. This is shown by the case of *o* Ceti where the line flux is relatively small for the unusually faint cycle in 1978 but much larger for the brighter maxima in 1982 (by a factor of ~100). Such a correlation is consistent with the idea that a stronger shock is formed in stronger (visually brighter) cycles, with an increase in ionization and related emission.

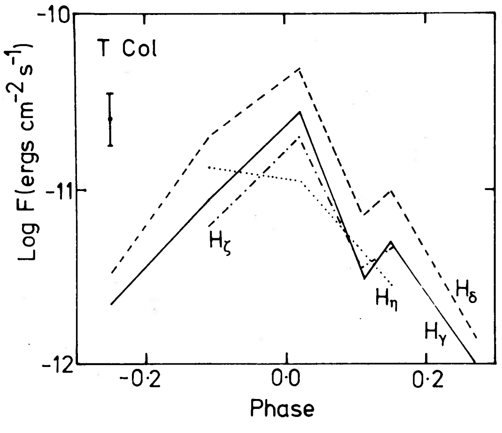

FIG. 14.—Absolute Balmer line flux plotted against phase in T Col.

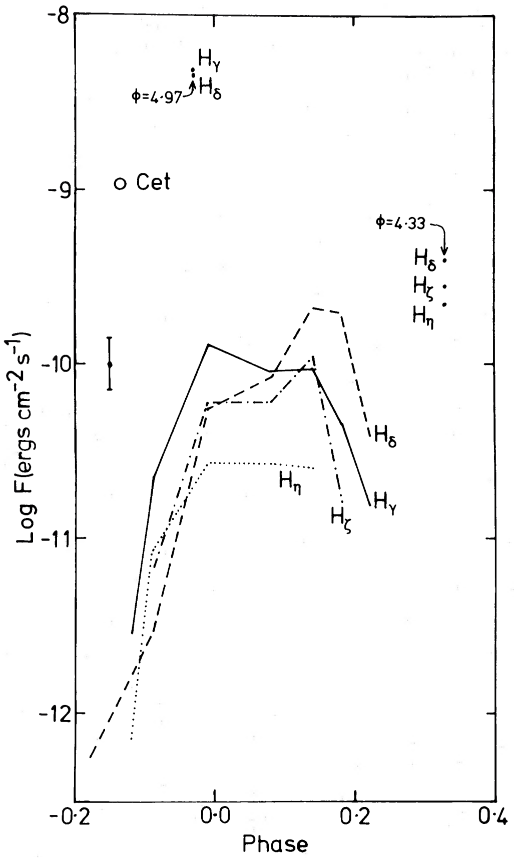

FIG. 15.—Absolute Balmer line flux plotted against phase in *o* Cet

Each of the Balmer lines Hγ, Hδ, Hζ, and Hη usually vary in a similar way in any given star. Differences observed can be largely attributed to mutilation of the lines by overlying absorption. For example, a well-correlated variation of fluxes can be seen in T Col (Fig. 14) where there is little discernible absorption past maximum light. In contrast, the relative intensity of the four lines in *o* Cet (Fig. 15) varies greatly over the faint 1978 cycle.

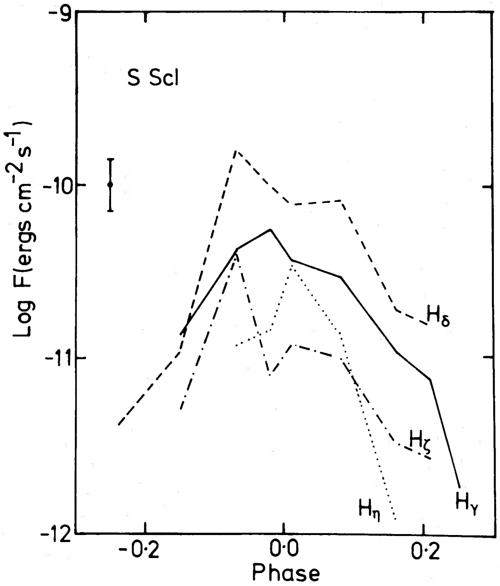

FIG. 16.—Absolute Balmer line flux plotted against phase in S Scl

A point of major interest is that line ratios, although somewhat uncertain, are not those of pure radiative recombination. In particular, Hγ/Hδ is typically around 0.7 in postmaximum phases when overlying absorption is not significant, as opposed to the value of 1.8 corresponding to Balmer emission in case B (the emission region optically thick to Lyα photons; Osterbrock 1974) when $T \approx 10{,}000$ K. Furthermore, the observed ratios Hζ/Hδ and Hη/Hδ ($\sim$0.7 and $\sim$0.4, respectively) are larger than the predicted values for pure recombination (0.4 and 0.3, respectively). There is no strong evidence to suggest that these ratios approach the pure recombination values out to phase 0.2 or even 0.3. The one exception to this is S Car, where the line ratio Hγ/Hδ of $\sim$1.45 is much closer to the pure recombination value.

V. A SIMPLE SHOCK MODEL

Comparisons of theoretical models of shock propagation in the outer layers of a Mira variable with the above data on absolute hydrogen emission line fluxes, line widths, and centers should yield powerful constraints on the hydrodynamic properties of Mira atmospheres. Here we present a simple picture of shock-related emission.

The velocity structure of a shock front in the rest frame of a typical Mira variable near maximum light is shown schematically in Figure 17. The preshock material consists of neutral and molecular hydrogen and helium with $T \approx 2500$ K infalling to the star at ~ 20 km s^{-1} (the quantitative values given here will be justified below). Immediately below the shock front, before the electron density has had time to build up sufficiently to cause significant ionization, is a region with $T \approx 34{,}500$ K and an outward velocity of ~ 5 km s^{-1}. The conditions in the immediate pre- and postshock regions are related by the Rankine-Hugoniot relations. Below the hot postshock region the burst of ionization occurs and below this again the ionized gas recombines, emitting Balmer and other line and continuum radiation. Assuming this emission is characterised by $T \approx 15{,}000$ K, the velocity at this point is ~ 9 km s^{-1} outward. Far behind the shock wave where the gas has cooled to $T \approx 4000$ K, the outward velocity is ~ 13 km s^{-1}. Velocities and temperatures in the various postshock regions are related to the immediate postshock values under the assumption that, in the frame of the shock front, ρv-constant, and there is no pressure gradient.

The velocities given above for pre- and postshock material can be deduced from the infrared Fourier transform spectroscopy of CO lines by Hinkle, Hall, and Ridgway (1982) and Hinkle, Scharlach, and Hall (1984). Around maximum light, the CO lines are split into two distinct velocity groups, one corresponding to cool infalling material and the other to warmer outflowing material. At this time, the shock front is passing through the region where the CO lines are formed, so that cool infalling material corresponds to the preshock region while the warm outflowing material corresponds to the far postshock region. From the plots of temperature against phase in Hinkle, Scharlach, and Hall (1984), typical temperatures of 2500 K and 4000 K can be deduced for the pre- and far postshock regions, respectively. By using the center-of-mass velocities given in Hinkle, Scharlach, and Hall, the velocities of pre- and postshock regions can be obtained. Typical observed values for the two regions are -15 and $+10$ km s^{-1}, respectively. Applying a correction factor to the observed velocities of

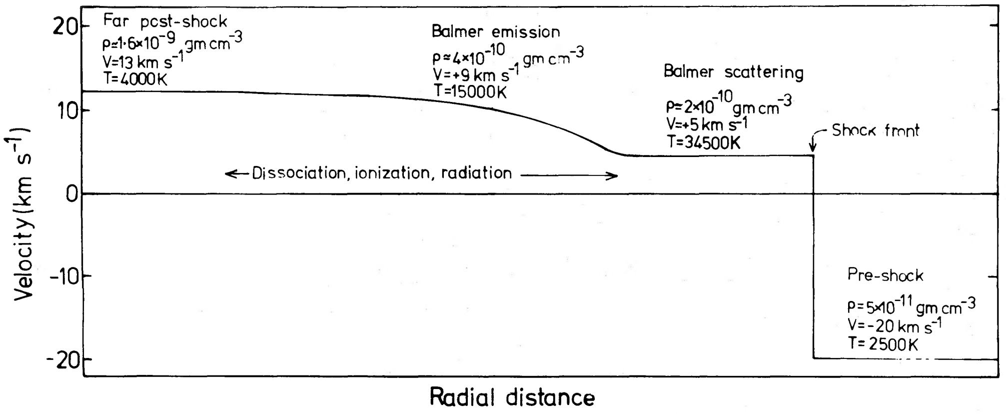

FIG. 17.—A schematic diagram of shock structure in a typical Mira variable near maximum light. Velocities are in the rest frame of the star.

1.3 to account for the fact that we are observing a limb-darkened disk yields true velocities for the pre- and far post-shock regions of about -20 km s^{-1} and $+12$ km s^{-1}, respectively.

The observed hydrogen line spectra can now be interpreted in terms of the model in Figure 17. As noted in § III, the hydrogen lines at early phase are very broad (full base widths of ~ 80 km s^{-1}), and they are centered roughly at the stellar center-of-mass velocity. At later phases, the hydrogen lines narrow, mainly because the negative velocity edge of the line decreases in intensity. We propose that the narrower line profiles seen at later phases are produced directly by photons emitted in the recombination region behind the shock, while the broad line profiles seen at early phases result from the scattering of Balmer photons by neutral hydrogen in the hot immediate postshock region. The excitation of hydrogen to the $n = 2$ level required for this latter process occurs either by electron collisions or by Lyα photons diffusing into this region from the recombination region behind. Note that the anomalous line ratios (e.g., Hγ/Hδ ~ 0.7) may also be explained by having a moderate optical depth to Balmer line radiation in the immediate postshock region. The scattering cross section is lower for higher order members of the Balmer series so that they will suffer less attenuation than lower order members. This will cause a reduction in line ratios such as Hγ/Hδ. Finally, we note that the weakening of the negative velocity emission component past maximum is due to the decrease in the scattering optical depth through the hot immediate postshock region.

Under the above assumptions, the broadening of the hydrogen lines is predominantly Doppler. For the four stars for which center-of-mass velocities can be found from maser and thermally excited microwave emission (see Table 1), Doppler line profiles have been fitted (1) to the broad base of Hδ (the line least affected by overlying absorption) at early phases to give an estimate of the temperature in the scattering region, and (2) to the top half of Hδ in the later phases to give an estimate of the temperature in the recombination region. Central line velocities have also been estimated for each line component. The temperatures and velocities so derived are shown as a function of phase in Figure 18. Around maximum, the temperatures indicated by the broad bases of the hydrogen lines are $\sim 30{,}000$ K, roughly that of the hot postshock region in Figure 17. Furthermore, the mean velocity of the broad emission component over the four stars is $+2$ km s^{-1}, not significantly different from the value of $(5 \div 1.3) \approx 4$ km s^{-1} given by the model in Figure 17. Similarly, the temperature derived for the recombination region averages around 15,000 K, while the velocity averages around 9 km s^{-1}, compared to the value of $(9 \div 1.3) \approx 7$ km s^{-1} expected from the model. Overall, the model appears to explain the Balmer emission-line spectrum very well.

The limb-darkening correction factor of 1.3 applied above to the emission-line velocities is very uncertain. For phases before or at maximum, the shock front is still within the photosphere so the back half of the expanding shock sphere will be occulted by the central star and will not contribute to the observed emission profile. Furthermore, the shock models of Fox and Wood (1984) indicate that Balmer line radiation emitted inward from the shock front is totally absorbed in the far postshock regions. This means that the far side of the expand-

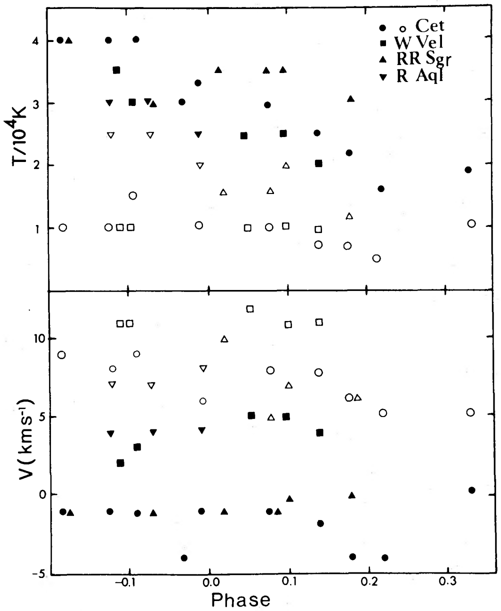

FIG. 18.—(*top panel*) Gas temperatures in the immediate postshock region (*solid symbols*) and the recombination region (*open symbols*) plotted against phase for the stars indicated. The temperatures are derived by fitting Doppler line profiles to the observed Balmer line profiles (see text for details). (*bottom panel*) the bulk velocity relative to the stellar center-of-mass of gas in the immediate postshock region as derived from the center of the broad base of Hδ (*solid symbols*) and of gas in the recombination region as derived from the center of the top half of the Hδ profile (*open symbols*).

ing shock sphere will not contribute to the observed emission-line profiles even at late phases when the shock front has passed well beyond the photosphere. In this situation, and in the absence of any overlying absorption, a geometric velocity correction factor of 1.5 (2.0) should be applied if the Balmer line emission region is optically thick (thin). However, model atmospheres for late-type stars (e.g., Manduca, Bell, and Gustafsson 1977) show that limb darkening (absorption within and above the photosphere) is large around 4000 Å, so that before and at maximum, a velocity correction factor of ~ 1.3 to account for limb darkening and projection effects is probably reasonable. For phases past maximum, the correction factor would be expected to increase due to the decrease in limb darkening as the shock rises above the bulk of the photosphere. This would lead to an increase with phase in observed emission-line strength at velocities between zero and the position of the existing line peak. However, such an effect is not observed, so that we have adopted a constant velocity correction factor of 1.3.

One factor not considered above is Stark broadening of the hydrogen lines. In order to evaluate the effect of Stark broadening, an estimate of electron density in the recombination region is needed; this also can be obtained from the results of Hinkle, Hall, and Ridgway (1982) and Hinkle, Scharlach, and Hall (1984). These authors give the column density of CO in Mira atmospheres as a function of phase. The column density of warm postshock material generally increases rapidly between phases 0.0 and 0.2 where it reaches a plateau. We interpret the rapid increase in column density up to phase 0.2 as being due mainly to the increase in physical depth of warm postshock gas in the CO-forming region as the shock moves through. The depth of the line-forming region at phase 0.2 can be obtained roughly by multiplying the outward velocity of the postshock region by the duration of shock traversal, $0.2 \times P$. The mean number density of CO molecules is then obtained by dividing the column density at phase 0.2 by the total depth of the line-forming region. Hydrogen densities and mass densities in the warm postshock gas can be obtained from the CO density by assuming that all C is locked up as CO and by adopting a solar C/H ratio in the M stars, and C/O = 1 in the S stars. This leads to a typical postshock density of 1.6×10^{-9} g cm^{-3} in the region where $T \approx 4000$ K. However, in the recombination region where $T \approx 15{,}000$ K, the density $\rho \approx 4.3 \times 10^{-10}$ g cm^{-3} (assuming zero pressure gradient in the postshock region). The thermal energy produced by the shock under consideration is sufficient to produce only $\sim 10\%$ ionization in the recombination region, so that the electron density there is $n_e \sim 1.9 \times 10^{13}$ cm^{-3}. By examination of the Stark-broadened line profiles in Vidal, Cooper, and Smith (1973), it can be seen that this electron density is an order of magnitude less than that required for any significant contribution of Stark broadening to the hydrogen line profile.

An interesting result evident in Figure 18 is that the immediate postshock temperature $T_{\rm ps}$ indicated by the solid symbols decreases uniformly with phase. Typical values are $T_{\rm ps} \approx 30{,}000$ K at phase $\phi = 0.0$, and $T_{\rm ps} \approx 20{,}000$ K at phase $\phi \approx 0.25$. For the strong shocks under consideration here, $T_{\rm ps} \propto v^2$, where v is the velocity of the shock relative to the preshock material. The decrease in postshock temperature between $\phi = 0.0$ and $\phi = 0.25$ thus indicates a decrease in shock velocity from ~ 34 km s^{-1} to ~ 28 km s^{-1} over the same interval, i.e., there is a significant slowing down of the shock with time after maximum light.

Finally we will comment on the observations of Mg I 4571 and the pumped lines Fe I 4202, 4307. In R Car at phase 5.15, Mg I 4571 is aligned ~ 5 km s^{-1} negatively with respect to the peak of the hydrogen lines. From Figure 17, we see that such a velocity coincides with that of the hot immediate postshock region, indicating that Mg I 4571 originates there. Note also that the Mg line falls at the center of the broad base of Hδ which we have previously suggested as originating in the immediate postshock zone. The negative velocity halves of the pumped Fe I lines seem to mirror the Mg I line in shape and velocity, and it is tempting to suggest that the immediate postshock region also produces the negative velocity halves of the pumped lines. The Fe lines also have a positive velocity extension, indicating that they are partially produced in a region with larger outflow velocity. The obvious region is the warm postrecombination region where the outflow velocity is larger (see Fig. 17). It is not unreasonable that the pumping photons (Mg II 2795) should excite Fe atoms both in front of and behind the recombination zone, their presumed region of production.

A major problem with the above picture is that the pumping line (Mg II 2795.53) is shifted by ~ 56 km s^{-1} relative to the pumped transition Fe I 2795.01. This large shift led Willson (1976) to postulate that the pumped lines were formed in the preshock material, which will be approaching the postshock Mg II emitting region at ~ 29 km s^{-1} in the model of Figure 17. A 29 km s^{-1} velocity shift will certainly help to bring the pumping and pumped transitions into alignment, but since the thermal velocities of Mg in the postshock material and Fe in the preshock region amount only to a few km s^{-1}, there is still a considerable discrepancy in wavelength.

The main problem with the idea that the pumped Fe lines come from the precursor region is that these lines do not have a negative velocity shift of ~ 29 km s^{-1} with respect to the Mg I lines as would be expected from the model. The problem of relative velocities could perhaps be overcome by postulating that Mg I was also formed in the preshock zone as a result of a precursor (note that Lyα with an energy of 10.2 eV is capable of ionizing Mg I with an ionization potential of 7.6 eV). However, the low electron density in the precursor region precludes any significant recombination of ionized species before passage of the shock. Thus formation of Mg I 4571 in the preshock is very unlikely; in addition, the (somewhat uncertain) mean velocity of Mg I of ~ 2 km s^{-1} does not indicate that this line is formed in the preshock zone infalling at about 20 km s^{-1}. Overall, the velocities indicate that the pumped Fe lines are formed in the postshock zone, but the difference in wavelength between the pumping and pumped transitions remains a problem.

The main reason for observing the Mg I 4571 and Fe I 4202, 4307 lines at the late phase of 4.53 in *o* Cet was to try to obtain information on the velocity of the shock at this time. However, the results for R Car show that the interpretation of velocities of these lines is not straightforward (a further complication in *o* Cet is the anomalous difference in the shape of the two lines Fe I 4202, 4307 as mentioned in § III*b*). The metal emission lines are centered at an outward velocity of $+4$ km s^{-1}. If this velocity is indeed representative of material in the current recombination region, then it indicates a considerable drop in velocity from the value of ~ 9 km s^{-1} obtained around maximum from the hydrogen lines.

Fitting of the emission line data to detailed shock models will be done in Paper II.

VI. SUMMARY

High-dispersion emission-line spectra and emission-line fluxes have been obtained for a number of Mira variables.

Before maximum, the hydrogen emission lines have full base widths of ~ 80 km s^{-1}, extending to ~ 40 km s^{-1} on either side of the stellar center-of-mass velocity. It is suggested that this broad emission results from scattering of Balmer line photons in the hot (3.5×10^4 K) immediate postshock region. After maximum, the negative (inward) velocity side of the hydrogen lines weaken due, it is suggested, to a decrease in the scattering optical depth of the hot immediate postshock region.

Around maximum, the velocities and temperatures (obtained from Doppler line widths) of the Balmer line emitting region are consistent with those of a simple shock model with parameters based on values expected from the results of high-dispersion infrared spectroscopy. Evidence for a slowing down of the shock with phase is provided by the time variation of the hydrogen emission-line widths and by the velocities of metal lines at late phases. A more detailed shock model is needed to deduce shock velocities as a function of phase from the phase variation of the Balmer emission-line fluxes.

REFERENCES

Bowers, P. F., and Kerr, F. J. 1977, *Astr. Ap.*, **57**, 115.
Breger, M. 1976, *Ap. J. Suppl.*, **32**, 7.
Catchpole, R. M., Robertson, B. S. C., Lloyd-Evans, T. H. H., Feast, M. W., Glass, I. S., and Carter, B. S. 1979, *South African Astr. Obs. Circ.*, No. 1, p. 61.
Fillit, R., Foy, R., and Gheudin, M. 1973, *Ap. Letters*, **14**, 135.
Fox, M. W., and Wood, P. R. 1984, in preparation (Paper II).
Gorbatskii, V. G. 1961, *Soviet Astr.*, **5**, 192.
Hauck, B., and Mermilliod, M. 1980, *Astr. Ap. Suppl.*, **40**, 1.
Hinkle, K. H. 1976, *Ap. J.*, **220**, 210.
Hinkle, K. H., Hall, D. N. B., and Ridgway, S. T. 1982, *Ap. J.*, **252**, 697.
Hinkle, K. H., Scharlach, W. W. G., and Hall, D. N. B. 1984, *Ap. J. Suppl.*, **56**, 1.
Hill, S. J., and Willson, L. A. 1979, *Ap. J.*, **229**, 1029.
Joy, A. H. 1947, *Ap. J.*, **106**, 288.
———. 1954. *Ap. J. Suppl.*, **1**, 13.
Keenan, P. C., Garrison, R. F., and Deutsch, A. J. 1974, *Ap. J. Suppl.*, **28**, 271.
Knapp, G. R., Phillips, T. G., Leighton, R. B., Lo, K. Y., Wannier, P. G., Wootten, H. A., and Huggins, P. J. 1982, *Ap. J.*, **252**, 616.
Kukarkin, B. V., *et al.* 1969, *General Catalogue of Variable Stars* (Moscow: Akademia Nauk).
Kurucz, R. L. 1979, *Ap. J. Suppl.*, **40**, 1.
Maehara, H. 1971, *Pub. Astr. Soc. Japan*, **23**, 313.
Manduca, A., Bell, R. A., and Gustafsson, B. 1977, *Astr. Ap.*, **61**, 809.
Merrill, P. W. 1945, *Ap. J.*, **102**, 347.
———. 1946*a*, *Pub. A.S.P.*, **58**, 304.
Merrill, P. W. 1946*b*, *Ap. J.*, **103**, 275.
———. 1947*a*, *Ap. J.*, **105**, 360.
———. 1947*b*, *Ap. J.*, **106**, 274.
Mihalas, D. 1966, *Ap. J. Suppl.*, **13**, 1.
Morris, M., Redman, M., and Reid, M. J. 1979, *Ap. J.*, **229**, 257.
Osterbrock, D. E. 1974, *Astrophysics of Gaseous Nebulae* (San Francisco: W. H. Freeman & Co.).
Reid, M. J., and Dickinson, D. F. 1976, *Ap. J.*, **209**, 505.
Robertson, B. S. C., and Feast, M. W. 1981, *M.N.R.A.S.*, **196**, 111.
Stapinski, T. E., Rodgers, A. W., and Ellis, M. J. 1981, *Pub. A.S.P.*, **93**, 242.
Thackeray, A. D., and Merrill, P. W. 1936, *Ap. J.*, **86**, 499.
Vidal, C. R., Cooper, J., and Smith, E. W. 1973, *Ap. J. Suppl.*, **25**, 37.
Willson, L. A. 1976, *Ap. J.*, **205**, 172.
———. 1982, in *Pulsations in Classical and Cataclysmic Variable Stars*, ed. J. P. Cox and C. J. Hansen (Boulder: Joint Institute for Laboratory Astrophysics Reprint), p. 269.
Willson, L. A., Wallerstein, G., and Pilachowski, C. A. 1982, *M.N.R.A.S.*, **198**, 483.
Wilson, W. J., and Barrett, A. H. 1972, *Astr. Ap.*, **17**, 385.
Wood, P. R. 1980, in *Physical Processes in Red Giants*, ed. I, Iben and A. Renzini (Dordrecht: Reidel), p. 205.
———. 1982, in *Pulsations in Classical and Cataclysmic Variable Stars*, ed. J. P. Cox and C. J. Hansen (Boulder: Joint Institute for Laboratory Astrophysics Reprint), p. 284.
Zirin, H. 1976, *Ap. J.*, **208**, 414.

M. A. Dopita, M. Fox, and P. Wood: Mount Stromlo and Siding Spring Observatories, Private Bag, Woden P.O., ACT 2626 Australia